LA-UR- 10-06900

Approved for public release;
distribution is unlimited.

Title:	Effect of debonded interfaces on corrosion of mild steel composites in supercritical CO2-saturated brines
Author(s):	Jiabin Han, J. William Carey and Jinsuo Zhang
Intended for:	NACE/2011, Houston, Texas. March 13-17, 2011

Los Alamos
NATIONAL LABORATORY
EST.1943

Effect of disbonded interfaces on corrosion of mild steel in supercritical CO_2 saturated brines

Jiabin Han
Earth and Environmental Sciences Division,
Los Alamos National Laboratory
Los Alamos, NM 87545
USA

James William Carey
Earth and Environmental Sciences Division,
Los Alamos National Laboratory
Los Alamos, NM 87545
USA

Jinsuo Zhang
Decision and Application Division, Los Alamos National Laboratory
Los Alamos, NM 87545
USA

ABSTRACT

The geologic sequestration of CO_2 is a proposed method to limit greenhouse gas emissions and has been the subject of many studies in the last decade. Wellbore systems achieve isolation of the storage reservoir through a combination of steel (generally carbon steel) and Portland cement. CO_2 leakage along the steel-cement interface has the potential to accelerate corrosion. We conduct experiments to assess the corrosion risk at cement-steel interface under *in situ* wellbore conditions. Wellbore interfaces were simulated by assemblies constructed of J55 mild steel and Portland class G (Epxoy was used in this study to sperate) cement and corrosion was investigated in supercritical CO_2 saturated brines, (NaCl=1 wt%) at T=50 °C, pCO_2=1200 psi with interface gap size = 100 μm and ∞ (open surface). The experiments were carried out in a high-pressure, 1.8 L autoclave. The corrosion kinetics were measured employing electrochemical techniques including linear polarization resistance and electrochemical impedance spectroscopy techniques. The corrosion scales were analyzed using secondary electron microscopy, back scattering electron microscopy, energy dispersive spectroscopy and x-ray diffraction. Corrosion rates decreased as time with or without interface gap. In this case corrosion rates are controlled by scale protectivity through the interface gap. Scaled steel corrosion rates were two orders of magnitude less compared with fresh steel. The corrosion scale is pseudo crystalline at the open interface. Well-crystallized scale was observed at interface gap sizes 100 μm. All corrosion scales were composed of iron carbonates.

Key words: Carbon dioxide, cement, corrosion, interface, surface analysis

INTRODUCTION

The geologic sequestration of CO_2 is a proposed method to limit greenhouse gas emissions and has been the subject of many studies in the last decade[1, 2]. The viability of CO_2 sequestration depends on the long-term performance of wellbore systems that must prevent buoyant supercritical CO_2 from escaping the storage reservoir. Wellbore systems achieve isolation of the storage reservoir through a combination of steel (generally carbon steel) and Portland cement. CO_2 leakage path development in cement has been widely investigated[3-9]. However, field analyses showed that the interfaces along the cement-caprock and cement-steel interfaces were more significant potential pathways for CO_2 leakage and are crucial to wellbore integrity[10-12]. In particular, CO_2 leakage along the steel-cement interface has the potential to accelerate corrosion. This issue has received very little attention, and in this paper, we conduct experiments to assess the corrosion risk at cement-steel interface under *in situ* wellbore conditions. Cement has two impacts to corrosion through alkalizing water chemistry and barring mass transfer. Preliminary results focus on its effect of mass transfer effect. This was achieved by substitute cement with inert epoxy.

EXPERIMENTAL PROCEDURE

Materials preparation

The epoxy-steel interface configuration used to investigate the effect of interface defect size on corrosion consisted of a coupon of epoxy and a coupon of embedded steel in epoxy separated by a gap created by inserting four pieces of Teflon tablet.

J55 steel coupon samples (2×1×0.5 cm^3) were manufactured from bulk tubing. A wire cable coated with insulating plastic was soldered on the coupon. The soldered joint was isolated from the environment by epoxy. The other five surfaces of the coupon were prepared by successively using 200 and 600 grit carbide sandpaper. The surfaces were cooled by spraying water during polishing. Finally, the surfaces were rinsed and ultrasonicated by high purity 2-propanol (purity >99.9%), and blown dry.

Steel samples were embedded in epoxy using molds with dimension 5×2.5×2.5 cm^3 and hardened for 20 hours at room temperature. After fully curing, the embedded steel samples were polished sequentially using 200, 600/1200 grit sandpaper to create a fresh steel surface. The fresh surface was ultrasonicated and blown dry. Same procedure was applied for a pure epoxy coupon. The two fresh surfaces of the epoxy and steel coupons were bound together with a gap created by inserting four Teflon tabs at the assembly corners. The Teflon tabs have thicknesses of 100 μm. An open interface was created by directly immersing steel fresh surface in corrosive environments.

Experimental design for electrochemical measurement in autoclave

A three electrode electrochemistry system was implemented in a Parr vessel autoclave facility. Three working electrodes (WE), J55 mild steel (Its composition is shown in Table 1), with a dimension of 1×2 cm^2 were installed in the autoclave. The corrosion potential was measured by referencing to a titanium rode electrode (RE). The autoclave body served as counter electrode. Cables connecting to WE and RE passed into the

autoclave through a compression fitting. Electrochemical techniques could be directly applied for monitoring corrosion behavior using any electrochemical instrument with a floating mode, e.g. Biologic SP-200 in this study.

Experimental procedure

The steel and steel-epoxy pair assemblies were immersed in the 1 wt% sodium chloride electrolyte solution (1 liter). The system was deaerated using CO_2 for at least one hour and heated to 50 °C. The autoclave was then pressurized to 100 bar by a booster pump. LPR (linear polarization resistance) and EIS (Electrochemical impedance spectroscopy) techniques were employed to in-situ measure the polarization resistance (by LPR), solution resistance (by EIS) and corrosion resistances (combining LPR and EIS). Solution resistance and corrosion resistance were fitted using EC-Lab software version 9.5.

Table 1. The chemical composition (weight percent) for J55 steel (provided by manufacturer)

Al	B	C	Ca
0.018	0.0001	0.36	0.0014
Cr	Cu	Mn	Mo
0.100	0.170	1.020	0.020
N	Nb	Ni	P
0.0099	0.001	0.070	0.007
S	Si	Sn	Ti
0.003	0.280	0.008	0.027
V	Fe		
0.002	balance		

Experimental test matrix

The corrosion conditions and electrochemical measurement parameters are listed in Table 2 and Table 3 respectively.

Table 2. Test conditions for the corrosion experiments

Interface material	Steel, Epoxy-steel
Interface gap size (μm)	100
Solution	1 wt% NaCl
Purge gas	CO_2
Temperature (°C)	50
Gas partial pressure (bar)	100
Bulk pH	3.1 (model calculation) [Error! Bookmark not defined.]
Test time (days)	7
Stirring speed (rpm)	0

LPR and EIS were employed to monitor corrosion kinetics. Their operational parameters are listed in Table 3. For LPR, the polarization potential was within ±10 mV *vs.* OCP (open circuit potential) at a

polarization speed of 0.1 mV/s. The frequency of AC for EIS was set between 0.01 Hz to 100 kHz. The sinus amplitude was 10 mV.

Table 3. Electrochemical measurement parameters for LPR and EIS

LPR	Polarization range (mV)	±10 *vs.* OCP
	Polarization speed (mV/s)	0.1
EIS	Frequecy range (Hz)	0.01 -200000
	Sample frequency (points/dec)	5
	Peak to peak voltage (mV)	10

RESULTS

Corrosion behavior

The corrosion rate monitored vs. time is sown in Figure 1. For open surface corrosion, the initial corrosion rate right after pressurization was about 10 mm/year. This observation agrees with literature reports[13, 14]. The current models predict much higher corrosion rate at the tested conditions[15, 16]. This indicates corrosion mechanism at supercritical pressure is different from the classic theory applied for low to moderate CO_2 pressure. Further investigation is required to understand corrosion mechanism at high pressure. Corrosion rate decreased as corrosion scale formed after a few hours and stabilized at a corrosion rate of two magnitudes lower. The initial fresh surface corrosion rate for open surface is ca. 10 times larger compared with 100 μm interface gap.

If the corrosion kinetics was controlled by interface gap, corrosion kinetics on open surface should be higher than that at 100 μm interface gap as observed at bare surface corrosion[17]. The final corrosion rates with the presence of corrosion scale are not dependent on epoxy-steel interface gap sizes. This is interpreted that corrosion kinetics was limited by the diffusion barrier, corrosion scale, instead of by interface gap of epoxy-steel.

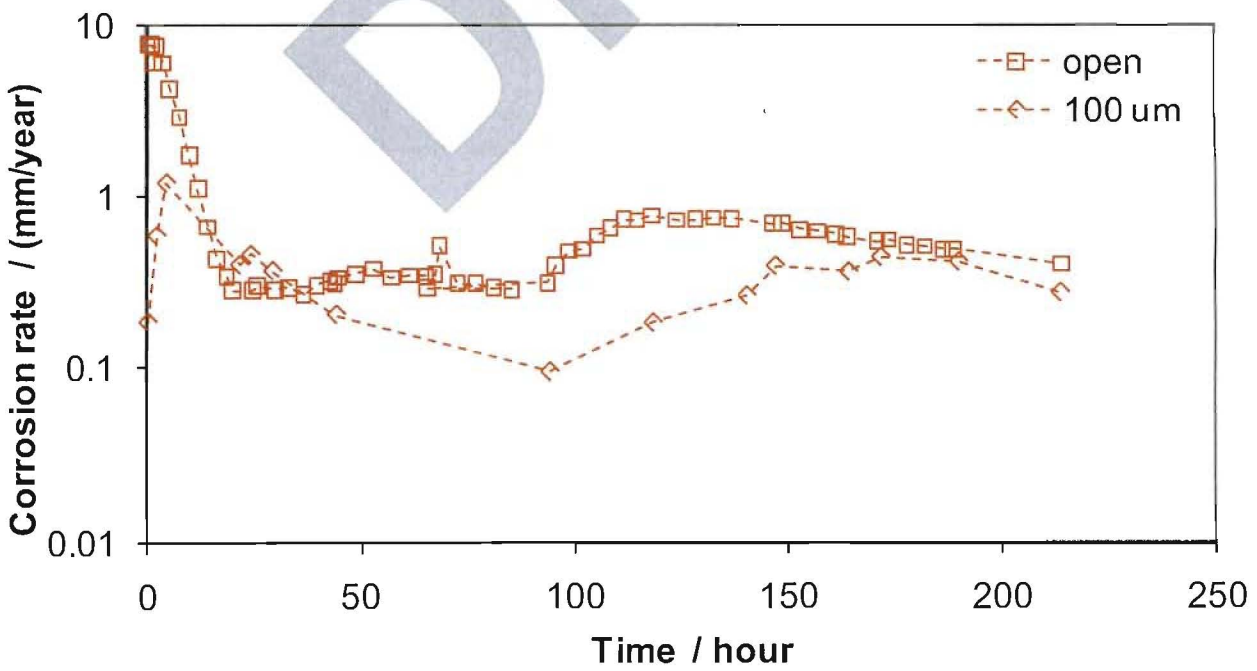

Figure 1 Corrosion history at open and 100 μm interface gaps at T=50 °C, p_{CO2}=100 bar, NaCl=1 wt%, stagnant flow.

The solution resistance (Figure 6) for open gap is one magnitude lower than that in 100 μm gap as expected. Electrons transfer is more difficult at limited space. Furthermore, the solution resistance is negligibly small compared with corrosion resistance, which accounts for 0.01% of corrosion resistance for open surface and 0.1% for 100 μm gap.

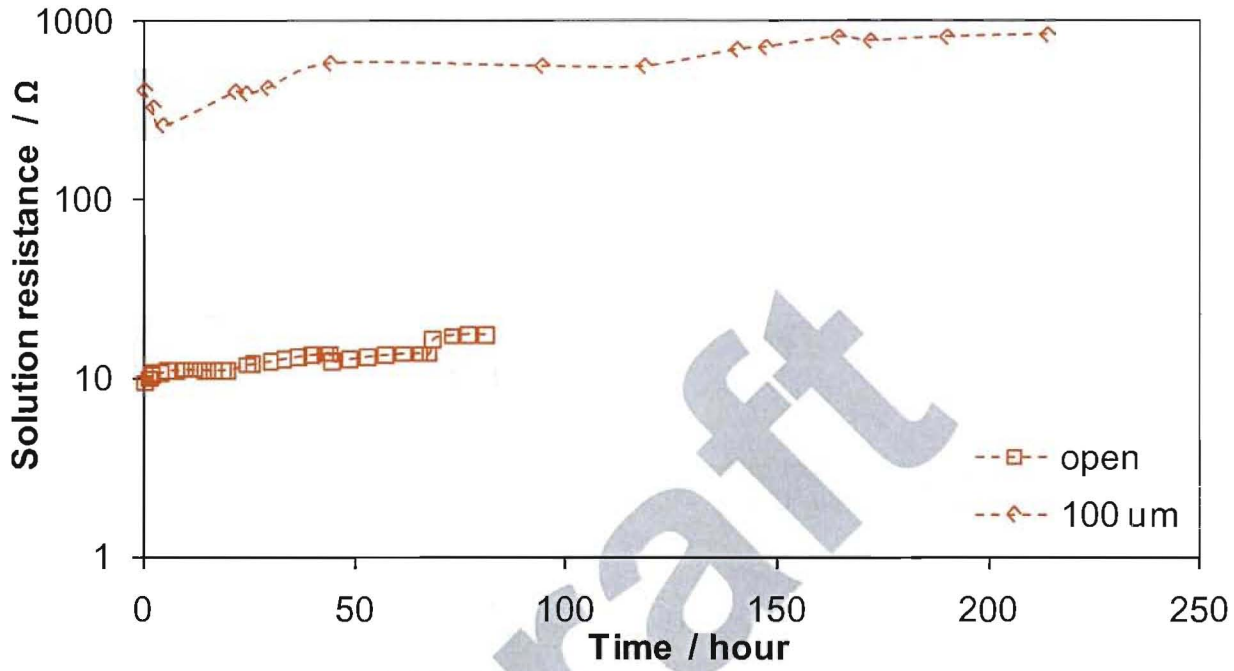

Figure 2 Solution resistance at open and 100 μm interface gaps at T=50 °C, p_{CO2}=100 bar, NaCl=1 wt%, stagnant flow.

At high CO_2 pressure, scale was formed on the corroding surface, as reflected by samples' weight gaining. The gained weight decreases as the interface gap decreases. The weight gained least for the sample mounted in the gas phase due to lack of water supply.

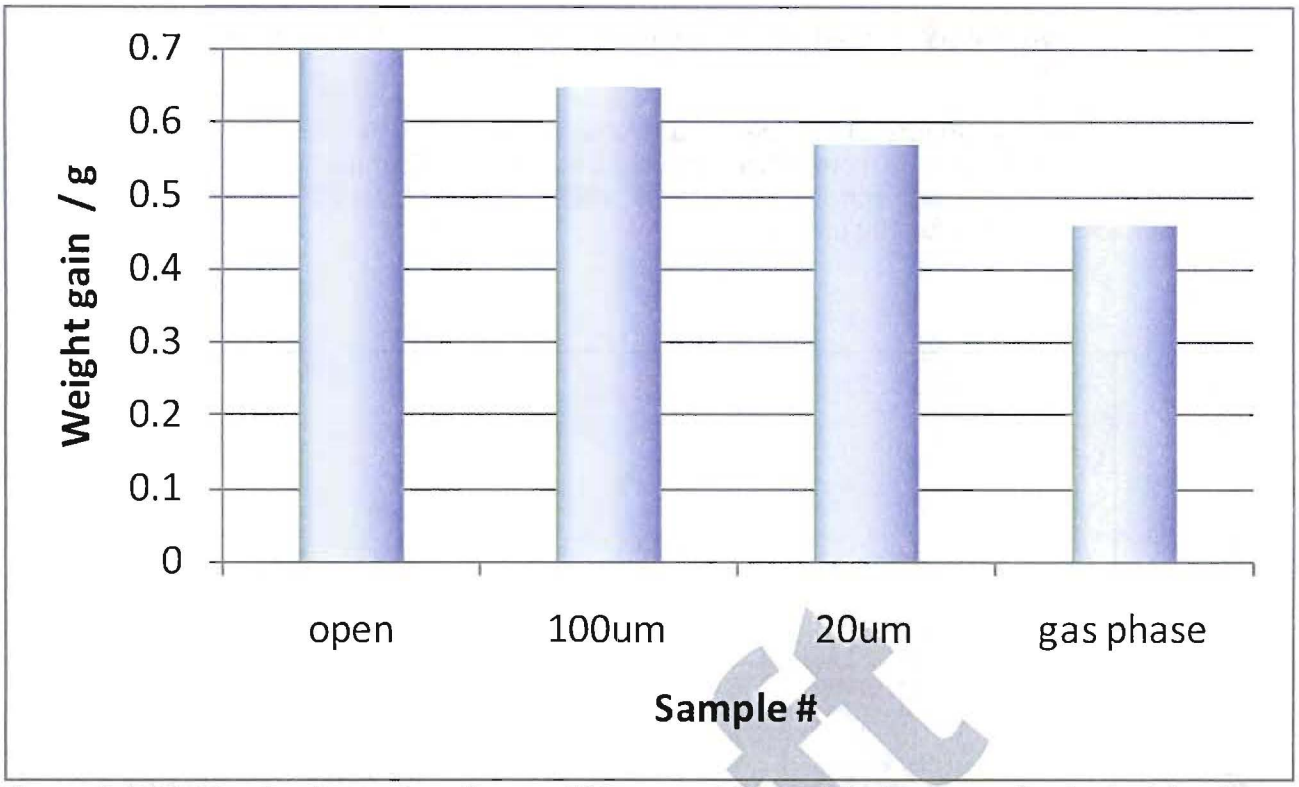

Figure 3 Weight gain of samples at open, 100 µm and 20 µm interface gaps in electrolyte phase and the one in gas phase at T=50 °C, p_{CO2}=100 bar, NaCl=1 wt%, stagnant flow.

Corrosion product analysis

Corrosion product morphology

The morphology of corrosion sample for open, 100 µm, 20 µm in electrolyte phase and the one in gas phase is shown in Figure 5.

From SEM picture of open surface corrosion, corrosion scale was detected on the surface. The polishing marks obviously remain. Carefully examining the corrosion morphology through BSE, crystal-like clusters interlocked inside of the carbide network. Considering the weight gain of samples for open surface is more than that at 100 µm gap. We can conclude that the scale grew more toward steel matrix and less outward of the electrolytes. BSE picture of cross-section (Figure 4a) shows that iron carbonate crystals are embedded in flocculent iron carbide network. This confirms that corrosion scale most grew toward steel matrix. This also tells that iron ions from the steel surface precipitates in the scale in a formation of carbonate without escaping to bulk solution.

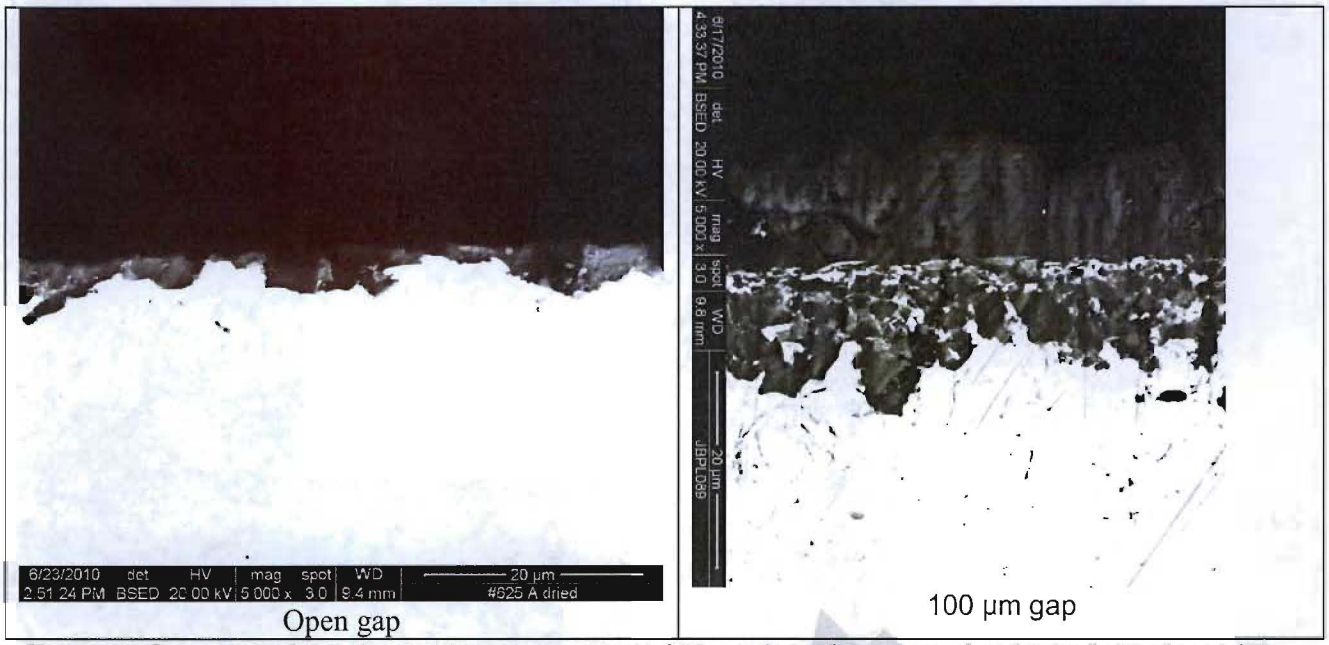

Figure 4 Cross section of samples at open and 100 µm interface gaps in electrolyte phase (The pictures were taken from a different batch of experiment at a similar condition as the current study).

At 100 µm gap, the corrosion product is compact crystals. This is because the initial corrosion rate is slower compared with open surface corrosion. A more moderate supersaturation was achieved on the steel surface, facilitating a fine crystal formation. BSE analysis of cross-section (Figure 4b) shows that corrosion scale grew toward both electrolyte and steel matrix directions. The corrosion protectivity of this scale is same as that formed on open surface. At 20 µm gap, the deficiency of mass supply due to the tiny passing path restricted the crystal growth, thus smallest crystals was formed in aqueous solution.

The corrosion morphology of corrosion scale in vapor saturated gas phase shows a petal-like texture. This is interpreted due to the corrosion in a condensed liquid drop out of the water vapor. At this circumstance, the crystal growth is minimum because of extreme shortage of corrosion reactant.

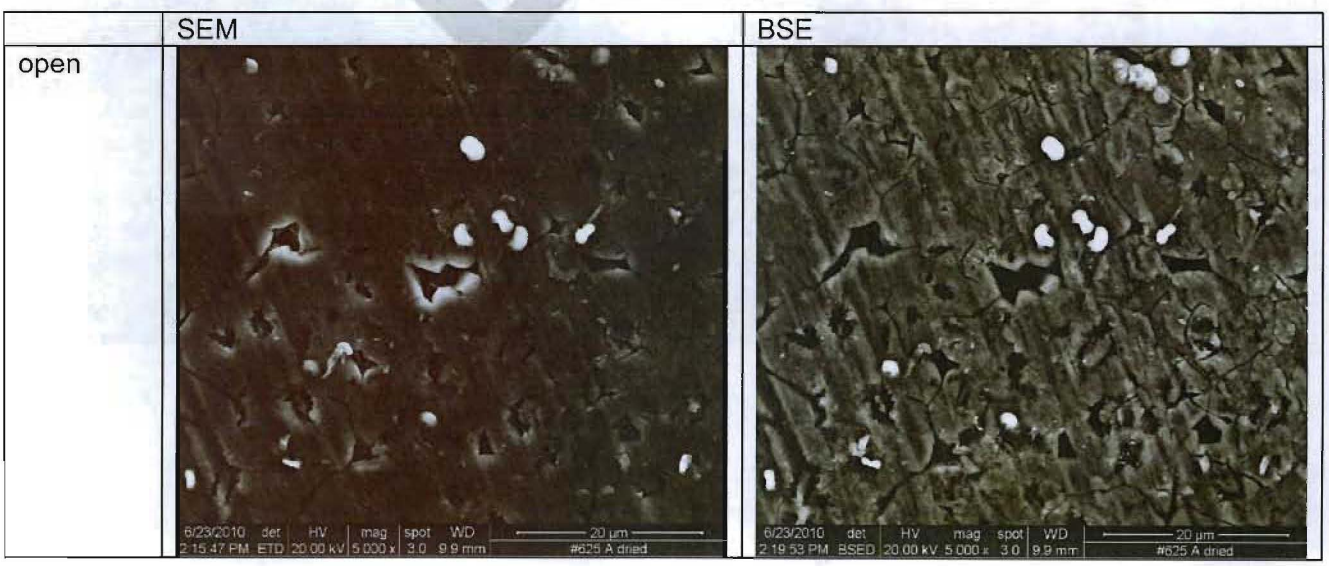

100 µm gap	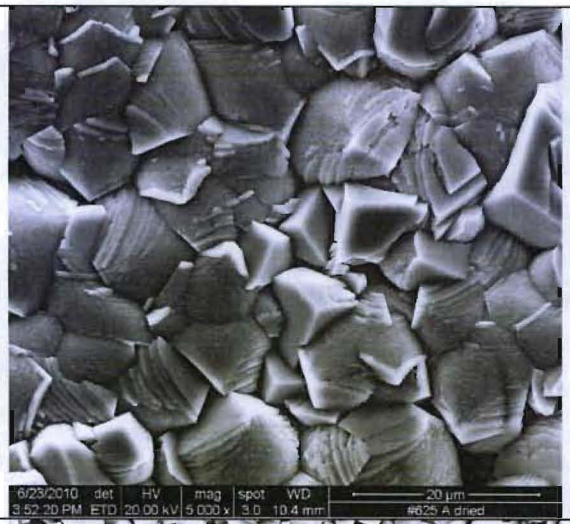	
20 µm gap		
Gas phase		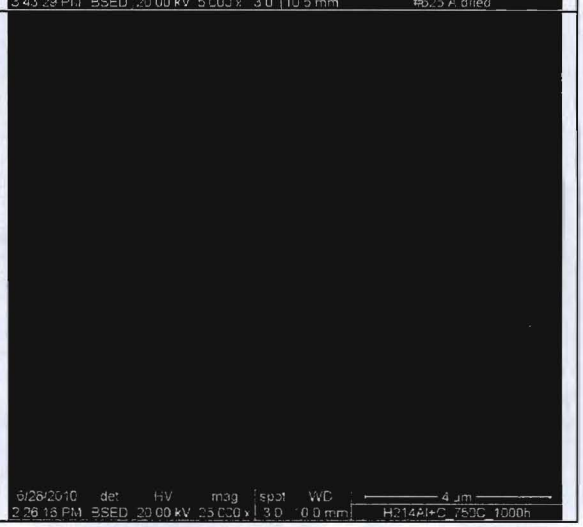

	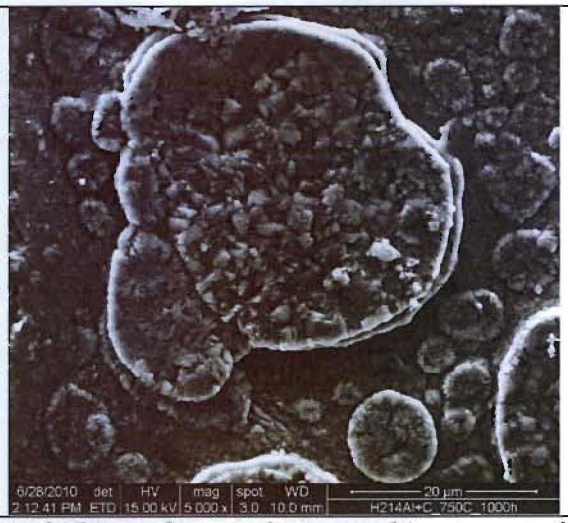	N/A

Figure 5 Morphology of corrosion samples at open, 100 µm, 20 µm interface gaps in liquid phase and the one in gas phase at T=50 °C, p_{CO2}=100 bar, NaCl=1 wt%, stagnant flow.

Corrosion product chemistry

EDX analysis data were collected and listed in Figure 6. Corrosion product on all surfaces is composed of iron, carbon and oxygen, indicating iron carbonate scale formation.

	Spot position	Spectroscopy	Composition
Open	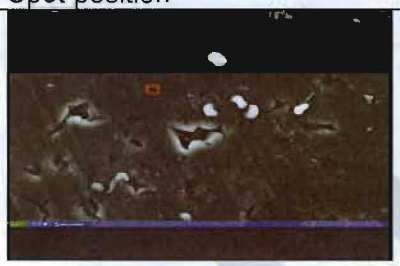	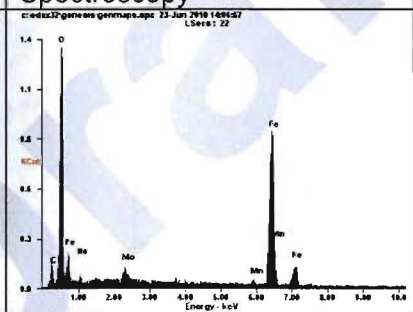	
100 µm		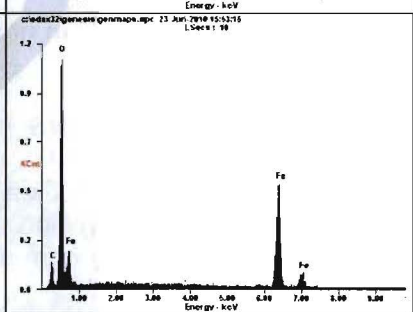	
Gas phase		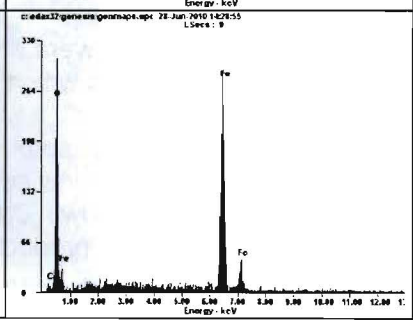	

Element	*Wt%*	*At%*
CK	09.28	17.77
OK	42.97	61.79
NaK	02.07	02.07
MoL	02.62	00.63
MnK	00.96	00.40
FeK	42.10	17.34
Matrix	Correction	ZAF

Element	*Wt%*	*At%*
CK	13.17	22.56
OK	49.56	63.72
FeK	37.27	13.73
Matrix	Correction	ZAF

Element	*Wt%*	*At%*
CK	03.53	08.35
OK	33.57	59.64
FeK	62.90	32.01
Matrix	Correction	ZAF

Figure 6 Solution resistance at open, 100 µm, 20 µm interface gaps in liquid phase and the one in gas phase at T=50 °C, p_{CO2}=100 bar, NaCl=1 wt%, stagnant flow.

To determine the corrosion product chemistry, XRD was carried out on sample surfaces (Figure 7). Only iron carbonate corrosion scale was detected. Iron signal originated from the steel matrix beneath the corrosion scale was observed.

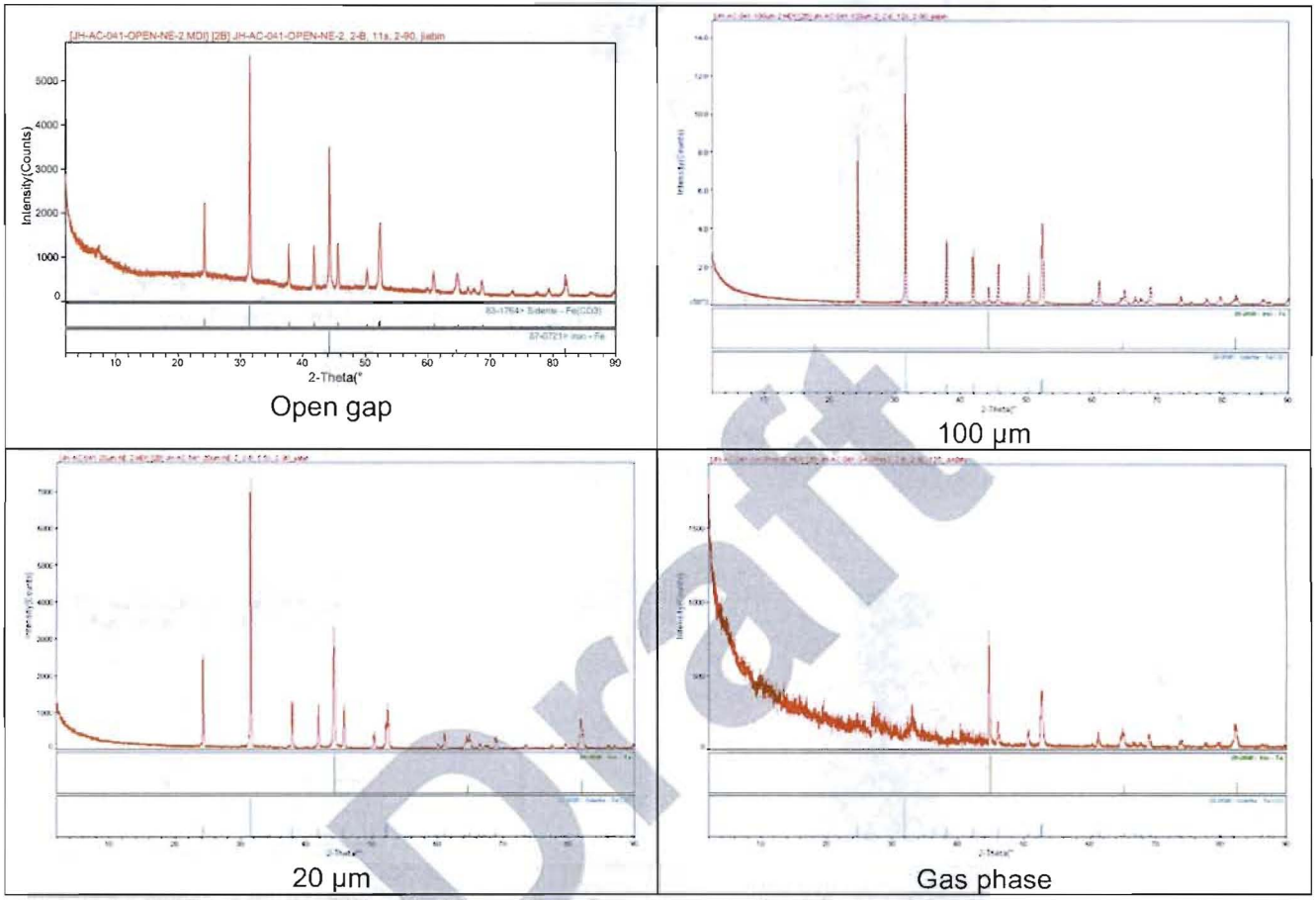

Figure 7 XRD at open, 100 µm, 20 µm interface gaps in liquid phase and the one in gas phase at T=50 °C, p_{CO2}=100 bar, NaCl=1 wt%, stagnant flow.

CONCLUSIONS

In this study, we investigated interface gap effect on corrosion and the scale properties. We discovered that current corrosion model predict much higher corrosion rate for initial corrosion rate immediately measured after pressurization. A need of identifying corrosion mechanism in aqueous supercritical CO_2 was proposed.

The final corrosion rates at the end of the experiments were same at open and 100 µm interface gap. The initial corrosion rates were dependent on gap sizes which acted as a mass transfer barrier.

Corrosion scale ($FeCO_3$) formation was observed at all samples. Pseudo-crystalline corrosion product was observed at open surface which was interlocked below surface level. The scale grew toward steel matrix for open surface corrosion and a mixed scale growth direction both toward solution and steel matrix was observed at 100 µm. A petal-like corrosion product, FeCO3, was observed on samples in

vapor saturated supercritical gas phase. The crystal size creased as the interface gap size became smaller.

ACKNOWLEDGEMENTS

The Fossil Energy program of the Department of Energy (FE-10-001) is acknowledged for funding support.

REFERENCES

1. S. Bachu, "Sequestration of CO_2 in geological media: criteria and approach for site selection in response to climate change", *Energy Conversion and Management*, 41, 9 (2000): 953-970.
2. S. Bachu, "Sequestration of CO_2 in geological media in response to climate change: road map for site selection using the transform of the geological space into the CO_2 phase space", *Energy Conversion and Management*, 43, 1 (2002): 87-102.
3. B. M. Huet, J. H. Prevost, G. W. Scherer, "Quantitative reactive transport modeling of Portland cement in CO_2-saturated water", *International Journal of Greenhouse Gas Control*, 4 (2010): 561–574.
4. Andrew Duguid, George W. SchererDegradation of oilwell cement due to exposure to carbonated brine, International Journal of Greenhouse Gas Control, 4 (2010): 546–560.
5. B. Kutchko, B. Strazisar, G. Lowry, D. Dzombak and N. Thaulow, "Degradation of Well Cement by CO_2 under Geologic Sequestration Conditions", *Environmental Science & Technology*, 41, 13 (2007): 4787-4792.
6. B. Kutchko, B. Strazisar, G. Lowry, D. Dzombak and N. Thaulow, "Rate of CO_2 Attack on Hydrated Class H Well Cement under Geologic Sequestration Conditions", *Environmental Science & Technology*, 42, 16 (2008): 6237–6242.
7. A. b. Sauki and S. Irawan, "Effects of Pressure and Temperature on Well Cement Degradation by Supercritical CO_2", *International Journal of Engineering & Technology IJET-IJENS*, 10, 04 (2010): 53-61.
8. I. Gaus, "Role and impact of CO_2–rock interactions during CO_2 storage in sedimentary rocks", *International Journal of Greenhouse Gas Control*, 4 (2010): 73–89.
9. J. Wollenweber, S. Alles, A. Busch, B.M. Krooss, H. Stanjek, R. Littke, "Experimental investigation of the CO_2 sealing efficiency of caprocks", *International Journal of Greenhouse Gas Control*, 4 (2010): 231–241.
10. J. W. Carey, M. Wigand, S. Chipera, G. WoldeGabriel, R. Pawar, P. Lichtner, S. Wehner, M. Raines and G. Guthrie, Jr., "Analysis and performance of oil well cement with 30 years of CO_2 exposure from the SACROC Unit, West Texas, USA", *International Journal of Greenhouse Gas Control*, 1, 1 (2007), 75-85.
11. W. Crow, J. W. Carey, S. Gasda, D. B. Williams, M. Celia, "Wellbore integrity analysis of a natural CO_2 producer", *International Journal of Greenhouse Gas Control*, 4, 2 (2010): 186-197.
12. J. W. Carey, R. Svec, R. Grigg, J. Zhang, W. Crow, "Experimental investigation of wellbore integrity and CO_2–brine flow along the casing–cement microannulus", *International Journal of Greenhouse Gas Control*, 4, 2 (2010): 272-282.
13. Sven Morten Hesjevik, Stein Olsen, Marion Seiersten: Corrosion at High CO2 Pressure. CORROSION/2003, Paper No. 03345, San Diego, 16-20 March 2003
14. Z.D. Cui, S.L. Wu, C.F. Li, S.L. Zhu, X.J. Yang, "Corrosion behavior of oil tube steels under conditions of multiphase flow saturated with super-critical carbon dioxide", Materials Letters, 58 (2004), p. 1035– 1040.
15. R. Nyborg, "CO_2 corrosion models in oil and gas production systems", NACE/2010, paper No. 10371, 2010
16. R. C. Woollam and S. E. Hernandez, "Assessment and comparison of CO_2 corrosion prediction models," Society of Petroleum Engineers, paper no. 100673, 2006.

17. J. Han, J. W. Carey and J. Zhang, "Assessing the Effect of Cement-Steel Interface Crevice on Well Casing Corrosion in Aqueous CO_2 Environments", 9th Annual Conference on Carbon Capture & Sequestration, (Pittsburg, PA. 2010).